ACS APPLIED MATERIALS & INTERFACES

Research Article

www.acsami.org

Synthesis, Characterization, and Application in HeLa Cells of an NIR Light Responsive Doxorubicin Delivery System Based on $NaYF_4$:Yb,Tm@SiO_2-PEG Nanoparticles

Paulino Alonso-Cristobal,[†] Olalla Oton-Fernandez,[†] Diego Mendez-Gonzalez,[†] J. Fernando Díaz,[‡] Enrique Lopez-Cabarcos,[†] Isabel Barasoain,[‡] and Jorge Rubio-Retama*[,†]

[†]Department of Physical-Chemistry II, Pharmacy Faculty, Complutense University of Madrid, 28040 Madrid, Spain

[‡]Department of Chemical and Physical Biology, Centro de Investigaciones Biológicas, Consejo Superior de Investigaciones Científicas, Ramiro de Maeztu 9, 28040 Madrid, Spain

Supporting Information

ABSTRACT: Herein, we present a phototriggered drug delivery system based on light responsive nanoparticles, which is able to release doxorubicin upon NIR light illumination. The proposed system is based on upconversion fluorescence nanoparticles of β-$NaYF_4$:Yb,Tm@SiO_2-PEG with a mean diameter of 52 ± 2.5 nm that absorb the NIR light and emit UV light. The UV radiation causes the degradation of photodegradable *ortho*-nitrobenzyl alcohol derivates, which are attached on one side to the surface of the nanoparticles and on the other to doxorubicin. This degradation triggers the doxorubicin release. This drug delivery system has been tested "*in vitro*" with HeLa cells. The results of this study demonstrated that this system caused negligible cytotoxicity when they were not illuminated with NIR light. In contrast, under NIR light illumination, the HeLa cell viability was conspicuously reduced. These results demonstrated the suitability of the proposed system to control the release of doxorubicin via an external NIR light stimulus.

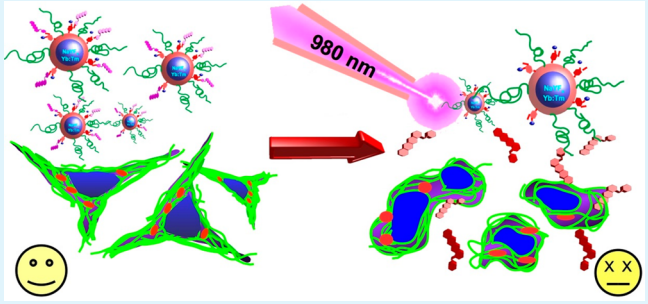

KEYWORDS: *doxorubicin, NIR light, upconversion, core@shell, phototriggered drug delivery*

1. INTRODUCTION

Stimuli responsive materials that undergo structural changes in response to external stimuli like pH,[1] temperature,[2] light,[3] etc., are of major interest due to their potential applications in electronics, photonics, and biomedicine. In the biomedical field, the use of nanomaterials capable of responding to external stimuli have emerged as ideal candidates to control and to monitor the drug release and to minimize the side effects associated with the use of certain drugs.[4−7] This is of special interest in cancer treatment, where the imbalance between potential risks and benefits leads to reject the use of toxic molecules that could serve as therapeutic tools if they were conveniently administered. This has prompted scientists to develop silenced drug delivery systems that can be activated on demand once they have reached the target tissue. For instance, the activation by means of alternating magnetic fields has been exploited as an interesting and versatile way to control the drug release.[8,9] Another interesting approach relies on the use of electric current to switch "on−off" the drug release.[10] However, the scarce capacity to localize with precision these stimuli into the target tissue has prompted scientists to use the light as an external stimulus to locally control the drug release. Initially, UV−vis[11] light was used to trigger the release of drugs after inducing conformational changes[12,13] solubility variations[14] or the photodegradation of a specific group.[15,16] However, *in vitro* studies demonstrated that the UV−vis light can be toxic for living cells since it is widely absorbed by tissue, diminishing the light penetration to a few microns. To solve these problems, NIR light has been used as an external stimulus, which coupled with plasmonic systems provokes a local temperature increment that ends up with the drug release.[17,18] An alternative to this approach has been recently described using upconversion nanoparticles. These particles can be considered as ideal candidates to transduce luminous signals into chemical signals that can trigger the drug release.[13,19,37]

The upconversion nanoparticles present a unique type of anti-Stokes fluorescence in which the excitation wavelength is higher than the emission wavelength.[20] In a typical upconversion process, two or more low-energy photons can be converted into a high-energy photon.[21] This process can occur in rare-earth doped $NaYF_4$ upconversion nanoparticles (UCNPs), which can absorb NIR light at a wavelength of 980 nm and emit UV−vis photons.[22−24]

Received: May 5, 2015
Accepted: June 21, 2015
Published: June 21, 2015

DOI: 10.1021/acsami.5b03881
ACS Appl. Mater. Interfaces 2015, 7, 14992−14999

Scheme 1. Synthesis Pathway of *4-(3-(Acryloyloxymethyl)-4-nitrophenoxy)butanoic Acid*

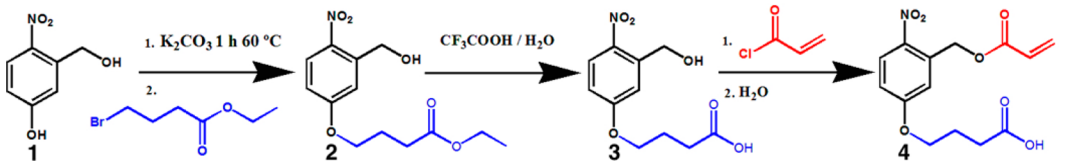

Among other examples, these upconverted photons have been used to photoactivate azobenzene (azo) groups anchored on the channels of the mesopore SiO_2 shell that covers UCNP nanoparticles. Upon NIR laser irradiation, the UV (350 nm) and visible (450 nm) light emitted by the UCNPs caused reversible cis−trans photoisomerization of the azo groups within the mesopore SiO_2, creating a continuous movement that triggers the release of chemotherapeutic molecules.[13]

Another interesting approach exploits the use of upconverted UV light to control the activation of pro-drugs. Thus, by combining Pt^{4+} compounds and UCNP nanoparticles it is possible to activate the Pt^{4+} pro-drug to a Pt^{2+} drug that kills the cells.[24]

Another possible strategy would involve the combination of upconverted light with photodegradable molecules[25] to create light responsive anchoring points that could release the drug upon the irradiation with UV light.[26,27] This strategy has been employed to release molecules such as acetic acid,[35] 5FU,[27] biomolecules,[19] or cells[16] by means of upconverted UV emission. However, this concept encloses several technical problems. The first one is the selection of the drug since it obliges to select highly potent drugs that require low concentrations to present therapeutic effects that can be observed by using a minimal amount of nanoparticles. Another major issue is the cytotoxicity of the system in the absence of the NIR light stimulus since the presence of drug-loaded nanoparticles could induce an uncontrolled therapeutic effect on the surrounding tissues. Finally, the attachment of the drug to the nanoparticles may require modifications of the chemical structure of the drugs. Such modifications can reduce their therapeutic effect, reducing the system efficacy. To prove the suitability of this NIR triggered drug release, it is necessary to board preliminary biological studies to test the system efficacy. These experiments are crucial to provide important information about the cytotoxicity of nonstimulated drug-loaded nanoparticles and about the therapeutic effect of the drug once it has been released by the NIR light stimulus. Therefore, these experiments could preliminarily determine the validity of the system for being used in real applications.

With the aim of addressing the above requirements, in this work we synthesize, characterize, and apply in HeLa cells a new doxorubicin delivery system that responds against NIR light. The phototriggered drug delivery system was based on UCNPs@SiO_2 nanoparticles, which have been functionalized with *ortho*-nitrobenzylalcohol derivate molecules (*o*-NBA). These photodegradable molecules anchored on the surface of the nanoparticles were used to covalently link doxorubicin (Dox), a potent cytotoxic drug. Upon NIR illumination, the Dox-loaded UCNPs@SiO_2 nanoparticles were able to release the drug. The amount of released drug was directly related with the illumination time, which indicated clearly that the drug was released due to the photodegradation mechanism.

Finally, to confirm the suitability of the system, we have carried out a parametric study on HeLa cells, where we have evaluated the cytotoxicity that UCNPs@SiO_2 nanoparticles and Dox-loaded UCNPs@SiO_2 nanoparticles exert in the presence or absence of NIR light stimulus. These results demonstrated the cytocompatibility of the doxorubicin loaded UCNPs@SiO_2 nanoparticles in the absence of luminous stimulus. By contrast, upon exposure to NIR light, the doxorubicin loaded UCNPs@SiO_2 nanoparticles showed their capacity to deliver the active drug reducing the HeLa cell viability. These results would pave the way for further applications in complex biological systems.

2. MATERIALS AND METHODS

2.1. Materials. Thulium(III) chloride hexahydrate (99.9%), ytterbium(III) chloride hexahydrate (99.9%), yttrium(III) chloride hexahydrate (99.99%), 1-octadecene (80%), oleic acid (90%), sodium hydroxide (98%), ammonium fluoride (98%), methanol (99.9%), *n*-hexane (95%), *N*,*N*-dimethylformamide anhydrous (DMF) (99.8%), tetraethyl orthosilicate (TEOS) (99.999%), polyoxyethylene (5) nonylphenylether, branched (IGEPAL CO-520), ammonium hydroxide solution (30%), (3-aminopropyl)triethoxysilane (APTES) (99%), *N*-(3-(dimethylamino)propyl)-*N*′-ethylcarbodiimide hydrochloride (EDC) (99%), *N*-hydroxysulfosuccinimide sodium salt (Sulfo-NHS) (98%), 5-hydroxy-2-nitrobenzyl alcohol (97%), ethyl 4-bromobutanoate (95%), acryloyl chloride (>97%), *O*-(2-aminoethyl)-*O*′-methyl-polyethylene glycol (Mw 5000 g/mol), and triethylamine (99.5%) (TEA) were purchased from Sigma-Aldrich and used as received. Doxorubicin hydrochloride (European Pharmacopoeia Reference Standard) was purchased from Sigma-Aldrich.

2.2. Characterization. Photoluminescence (PL) spectra were collected using a JASCO spectrofluorometer. Absorption spectra were taken with a Varian Cary 300 Bio UV−vis spectrophotometer. ^{1}H NMR spectra were collected using a Bruker AVANCE 250 MHz NMR spectrometer. FT-IR spectra were acquired using a Thermo Nicolet 200IR spectrometer. Transmission electron microscopy (TEM) studies were carried out using and a JEOL JEM 1010 operated at 80 kV. EDX analysis was performed using a JEOL JEM2100 with 200 kV of acceleration voltage. TEM samples were prepared by placing a drop of diluted solutions of the nanoparticles on a Formvar coated copper grid. Z-potential experiments were carried out using a Malvern Nano-ZS system equipped with a He−Ne laser working at 632.8 nm. X-ray diffraction patterns (XRD) of the UCNP particles were collected using a Philips X'pert.

3. EXPERIMENTAL SECTION

3.1. Synthesis of the Photodegradable Anchoring Molecule. The photodegradable linker based on *4-(3-(acryloyloxymethyl)-4-nitrophenoxy)butanoic acid* (*o*-NBA) was synthesized in several steps that are schematically depicted in Scheme 1.

The synthesis of the photodegradable linker is described as follows:

3.1.1. Ethyl 4-(3-(Hydroxymethyl)-4-nitrophenoxy)butanoate (2). 5-Hydroxy 2-nitrobenzyl alcohol (1 g, 6 mmol) and potassium carbonate (2.1 g, 15 mmol) were dissolved in 10 mL of DMF at 60 °C. After 1 h, ethyl 4-bromobutanoate (1 mL, 6 mmol) was added dropwise and stirred overnight. The solution was then poured into water (300 mL), stirred for 1 h, and cooled to 5 °C for 2 h. The resultant precipitate was filtered and washed with water. The product was a yellow solid (1.4 g, 5 mmol, 83%). The ^{1}H NMR is depicted in Figure S1.

3.1.2. 4-(3-(Hydroxymethyl)-4-nitrophenoxy)butanoic Acid (3). *Ethyl 4-(3-(hydroxymethyl)-4-nitrophenoxy)butanoate (1.4 g, 5 mmol)* was stirred in a solution of water (10 mL) and trifluoroacetic acid (1

DOI: 10.1021/acsami.5b03881
ACS Appl. Mater. Interfaces 2015, 7, 14992−14999

mL) at 60 °C overnight. The solution was allowed to cool to room temperature resulting in the formation of pale yellow precipitate. The precipitate was filtered and recrystallized in water to yield pale yellow crystals (1.01 g, 4 mmol, 81%). The ^{1}H NMR is depicted in Figure S1.

*3.1.3. 4-(3-(Acryloyloxymethyl)-4-nitrophenoxy)butanoic Acid (**4**).* *4-(3-(Hydroxymethyl)-4-nitrophenoxy)butanoic acid* (1 g, 4 mmol) and TEA (1.25 mL, 9 mmol) were dissolved in THF (25 mL) and then cooled to 0 °C with an ice bath. Acryloyl chloride (0.7 mL, 9 mmol) in anhydrous THF (10 mL) was added dropwise, and the mixture was allowed to react overnight. The solution was filtered out to remove the TEA salts. Next, 250 mL of water was added, and the solution was transferred to a separation funnel, where the product was extracted with DCM (40 mL) × 3. Finally, the product was dried under vacuum to obtain an amber viscous liquid (0.660 g, 2.1 mmol, 53%). The ^{1}H NMR is depicted in Figure S1.

3.2. Synthesis of the Doxorubicin Functionalized β-NaYF$_4$:Yb,Tm@SiO$_2$ Nanoparticles. *3.2.1. Synthesis of β-NaYF$_4$:Yb,Tm Nanocrystals.* The synthesis of monodisperse β-NaYF$_4$:Yb$_{0.244}$,Tm$_{0.046}$ nanoparticles was carried out by following a previously reported procedure.[28] In a typical synthesis, yttrium(III) chloride hexahydrate (236.62 mg, 0.78 mmol), ytterbium(III) chloride hexahydrate (77.5 mg, 0.20 mmol), and thulium chloride hexahydrate (1.1 mg, 0,003 mmol) were dissolved in a three-neck round-bottom flask with oleic acid (6 mL, 19 mmol) and 1-octadecene (15 mL, 46.9 mmol) and heated at 160 °C for 2 h under nitrogen atmosphere. After that the temperature was cooled to 50 °C. Then, a solution of sodium hydroxide (100 mg, 2.5 mmol) and ammonium fluoride (148.16 mg, 4 mmol) dissolved in 10 mL of methanol was added dropwise in the reaction media under vigorous stirring. The mixture was slowly heated to 100 °C for 2 h under N_2 atmosphere and then 30 min under vacuum. Next, the solution was heated to 300 °C under an argon atmosphere for 1.5 h. After this time the reaction was cooled, and the β-NaYF$_4$:Yb,Tm nanoparticles were collected by centrifugation (8500 rpm, 10 min) with a mixture of hexane, ethanol, and water (2:1:1 in volume). The pellet was dispersed with 5 mL of ethanol and centrifuged in a mixture of ethanol and water (1:1 v/v). This process was repeated three times. Finally, the purified NaYF$_4$:Yb,Tm nanoparticles were dispersed and stored in hexane.

*3.2.2. Synthesis of Silica-Coated β-NaYF$_4$:Yb,Tm Nanocrystals (**1**).* The silica coating of the synthesized UCNPs was performed by the base catalyzed polymerization of TEOS in a reverse microemulsion.[29,30] Briefly, 240 mg, 0.5 mmol of IGEPAL CO-520, and 5 mL of a hexane solution with the UCNPs (2 mg/mL) were mixed with an ultrasound bath. Then, an ammonium hydroxide solution (40 μL, 30%) was added and gently mixed. The solution turned totally transparent, which indicated the formation of the microemulsion. The reaction started when TEOS (30 μL, 0.14 mmol) was added under stirring, and it was left to react overnight at room temperature. The reaction finished when the microemulsion was destabilized with 5 mL of methanol. The core@shell (β-NaYF$_4$:Yb,Tm@SiO$_2$) nanoparticles (UCNP@SiO$_2$) were purified by centrifugation (3 × 8500 rpm, 10 min) with ethanol.

*3.2.3. Synthesis of Amine Functionalized β-NaYF$_4$:Yb,Tm@SiO$_2$ Nanoparticles (**2**).* The amine functionalized β-NaYF$_4$:Yb,Tm@SiO$_2$ nanoparticles (UCNP@SiO$_2$-NH$_2$) were prepared as previously described:[31] The as-synthesized UCNP@SiO$_2$ nanoparticles were dispersed in 5 mL of ethanol, and 150 μL of APTES (0.68 mmol) was added. This mixture was stirred at room temperature overnight. The UCNP@SiO$_2$-NH$_2$ nanoparticles were centrifuged (3×) and dispersed in 5 mL of anhydrous THF.

3.2.4. Attachment of PEG Chains on the Surface of the UCNPs@SiO$_2$. With the aim of providing colloidal stability to the amine functionalized NaYF$_4$:Yb,Tm@SiO$_2$ nanoparticles, methoxypolyethylene glycol (Mw 5000) chains were attached to the surface of the nanoparticles. This was achieved through several steps as follows:

3.2.4.1. Synthesis of Methoxypolyethylene Glycol Carboxylic Acid. *O*-(2-Aminoethyl)-*O*′-methyl-polyethylenglycol (500 mg, 0.1 mmol), triethylamine (100 μL, 1 mmol), and succinic anhydride (100 mg, 1 mmol) were dissolved in THF and heated to reflux overnight. After that, the product of this reaction was dried using a rotary evaporator, and then it was dissolved in water. Subsequently, the methoxypolyethylene glycol carboxylic acid was extracted with CH_2Cl_2 using a separation funnel.[32]

3.2.4.2. Attachment of the Methoxypolyethylene Glycol Carboxylic Acid on the Surface of the NaYF$_4$:Yb,Tm@SiO$_2$ Nanoparticles. Methoxypolyethylene glycol carboxylic acid (25 mg, 5 × 10^{-3} mmol) was dissolved in 5 mL of a PBS solution (0.1 M sodium phosphate, NaCl, 0.15 M, pH 7.3) prior to the addition of an EDC solution in PBS (100 μL, 0.2 M) and a solution of Sulfo-NHS (200 μL, 0.2 M) in PBS. This mixture was stirred for 10 min. After that, 5 mL of a PBS solution containing 25 mg of amine functionalized NaYF$_4$:Yb,Tm@SiO$_2$ nanoparticles was added. The reaction mixture was stirred overnight at room temperature. The NaYF$_4$:Yb,Tm@SiO$_2$-PEG nanoparticles were purified by centrifugation (10.000 rpm, 20 min) three times and stored in the refrigerator.

*3.2.5. Attachment of the Photodegradable Linker Molecule on the Surface of the NaYF$_4$:Yb,Tm@SiO$_2$-PEG Nanoparticles (**4**).* EDC (25 mg, 0.15 mmol) and sulfo-NHS (50 mg, 0.28 mmol) were mixed with *4-(3-(acryloyloxymethyl)-4-nitrophenoxy)butanoic acid* (25 mg, 0.08 mmol) in 5 mL of DMF. This mixture was stirred for 10 min, and, after this time, 25 mg of NaYF$_4$:Yb,Tm@SiO$_2$-PEG nanoparticles dispersed in 5 mL of DMF was poured. The reaction mixture was stirred overnight at room temperature and purified by centrifugation at (10000 rpm, 20 min) twice. The nanoparticles were dissolved in 5 mL of Milli-Q water and stored in the refrigerator.

*3.2.6. Attachment of Doxorubicin on the Photodegradable 5-Hydroxyl 2 Nitrobenzyl Alcohol Anchored on the Surface of NaYF$_4$:Yb,Tm@SiO$_2$-PEG Nanoparticles (**5**).* The attachment of Dox on the surface of the particles was performed by using the thiol−acrylate Michael addition reaction.[33] Prior to perform this coupling reaction, Dox was thiolated according to a previously reported method.[34] Briefly: 2-iminothiolane hydrochloride (2-IT, 1 mM, 250 μL) and Dox (0.5 mM, 300 μL) were mixed at room temperature for 20 min. Then 5 mL of the previously obtained NaYF$_4$:Yb,Tm@SiO$_2$-PEG nanoparticles (25 mg) was mixed with the thiolated Dox solution and left to react overnight. The product was centrifuged at 14 000 rpm for 20 min, and the precipitate was washed three times with Milli-Q water, alternating centrifugation and redispersion in an ultrasonic bath in order to remove any unbound Dox. After the cleaning process, the red precipitate was collected and stored in the dark for further experiments.

3.3. Calculating the Doxorubicin Loading Capacity of the Nanoparticles. To determine the amount of Dox loaded on the surface of the nanoparticles, 4 mg of Dox-UCNP@SiO$_2$ was poured in 2 mL of Milli-Q water, which contained 0.1 mL of HF (35% w/w). This solution was stirred for 24 h at r.t. After that, the absorbance was measured with UV−vis at 480 nm and compared against a calibration curve of Dox under the same conditions. The calibration curve is shown in Figure S4. The inset shows the UV−vis curves of the different Dox concentrations (red curves) and the curve obtained from the sample (black curve). From this result, we inferred that the Dox payload of the nanoparticles was 1.4% (w/w).

3.4. NIR Light Irradiation Experiments. A CW 980 nm laser (Armlaser USA) was used to irradiate the nanoparticle dispersion and the 96 well plates. The power of the NIR laser beam at the sample was set as 6.3 W/cm^2.

3.4.1. Phototriggered Release of Dox. The phototriggered release of Dox in solution was done by mixing 7 mg of Dox-UCNP@SiO$_2$ with 7 mL of PBS buffer solution. This mixture was divided in seven aliquots. Each of these aliquots was irradiated with a 980 nm NIR laser for different periods of time at a fixed power density of 6.3 W/cm^2 and an exposition area of 0.5 cm^2. After that, the samples were centrifuged, and the released Dox content was analyzed from the supernatant of each sample. A control experiment was done following the same methodology but without any NIR irradiation. The release profile of Dox molecules was quantified by monitoring the increasing fluorescence signals at 590 nm, and it was represented as a function of the exposure time.

3.4.2. Cell Culture and Cytotoxicity Assays. Human HeLa cervix carcinoma cells were continuously maintained in DMEM supple-

DOI: 10.1021/acsami.5b03881
ACS Appl. Mater. Interfaces 2015, 7, 14992−14999

Scheme 2. Synthetic Pathway Used in the Preparation of the NIR Light Responsive Drug Delivery System

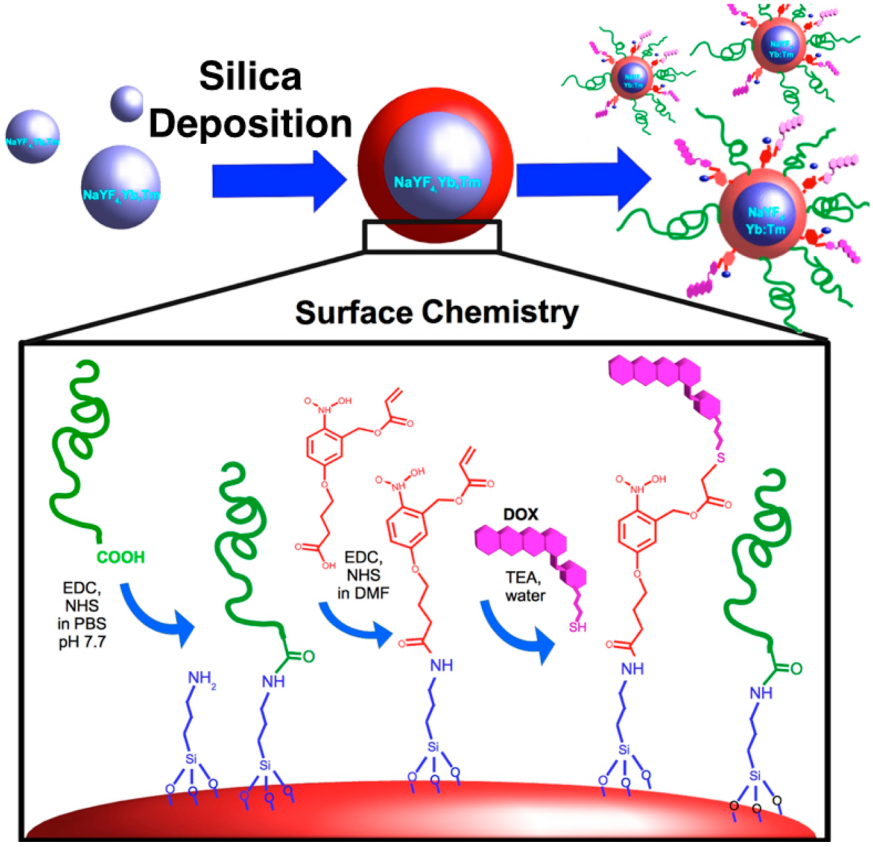

mented with 10% fetal calf serum, 2 mM L-glutamine, 40 μg mL^{-1} gentamycin, 100 IUL^{-1} penicillin, and 100 μg mL^{-1} streptomycin. Cytotoxicity of Dox-UCNP@SiO_2 nanoparticles was assayed against HeLa cells. Cells were seeded in a 96-well plate at a density of 9600 cells in 0.08 mL per well and cultured in 5% CO_2 at 37 °C for 24 h. Then, the Dox-loaded UCNP@SiO_2 nanoparticles were plated on top of the cell layer at different concentrations and exposed to the 980 nm laser for 5 min at a power density of 6.3 W/cm^2. Several controls were included with the aim of differentiating the influence of each part of the system in the cell viability: (i) Dox-loaded nanoparticles were plated at the same concentrations but not exposed to the stimulus, (ii) UCNP@SiO_2 nanoparticles without Dox were plated at the same concentrations and treated with and without the 980 nm laser radiation for 5 min, which would determine the influence of the emitted UV photons from the sample on the cell viability and (iii) 5 min radiation to untreated cells to test the influence of the laser beam on the cell viability. After the addition of the nanoparticles and the exposure to the stimulus, the cells were incubated in 5% CO_2 at 37 °C for an additional 48 h. Cell viability was determined with a modified MTT assay. For this purpose, 20 μL of 2.5 mg mL^{-1} of 3-(4,5-dimethylthiazol-2-yl)-2,5-diphenyltetrazolium bromide (MTT) was added to each well, incubated for 4 h at 37 °C, and then treated with 0.1 mL of MTT solubilizer (10% SDS, 45% dimethylformamide, pH 5.5). Plates were again incubated overnight at 37 °C in order to solubilize the blue formazan precipitate before measuring the absorbance at 595/690 nm in an automated Appliskan microplate reader. Control wells containing medium without cells were used as blanks. The MTT response is expressed as a percentage of the control (untreated) cells. The IC_{50} was calculated from the log−dose response curves. All these experiments were performed in triplicate, and the results are represented with the media and the standard deviation.

4. RESULTS AND DISCUSSION

The synthetic process is represented in Scheme 2.

The as-synthesized nanoparticles were hexagonal crystals with an average length of 43 ± 1.5 nm and a mean width of 38 ± 1.2 nm, as shown in Figure 1A. The X-ray Diffraction (XRD)

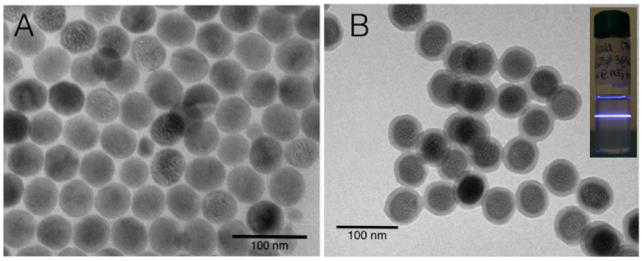

Figure 1. A) TEM image of the UCNPs before the silica coating. B) TEM image of UCNP@SiO_2 nanoparticles. The inset shows the UV−vis emission of the UCNP@SiO_2-PEG under 980 nm laser excitation.

pattern of the UCNPs was successfully indexed to the hexagonal β-$NaYF_4$ phase (JCPDS standard card 16-0334), Figure S2B. The EDX analysis confirmed that the synthesized nanoparticles were β-$NaYF_4$:Yb,Tm, see Figure S2D.

The silica coating reaction permitted to grow a SiO_2 shell on the surface of the UCNP nanoparticles with a thickness of 8.5 ± 0.5 nm, see Figure 1B. The deposition of the SiO_2 shell permitted introducing functional groups that allowed further surface modifications.[29] After this step the UCNP@SiO_2 nanoparticles were treated with APTES to incorporate amine groups. The Z-potential of the UCNPs@SiO_2 nanoparticles turned from −26.5 ± 2.85 mV to +9.14 ± 2.49 mV, which was indicative of the presence of NH_2 groups on the surface of the nanoparticles.

DOI: 10.1021/acsami.5b03881
ACS Appl. Mater. Interfaces 2015, 7, 14992−14999

To provide colloidal stability and stealth properties, PEG chains were grafted on the surface of the UCNP@SiO_2 nanoparticles. This modification was followed by FTIR, see Figure 2A. The FTIR spectrum of the pristine NaYF4:Yb,Tm

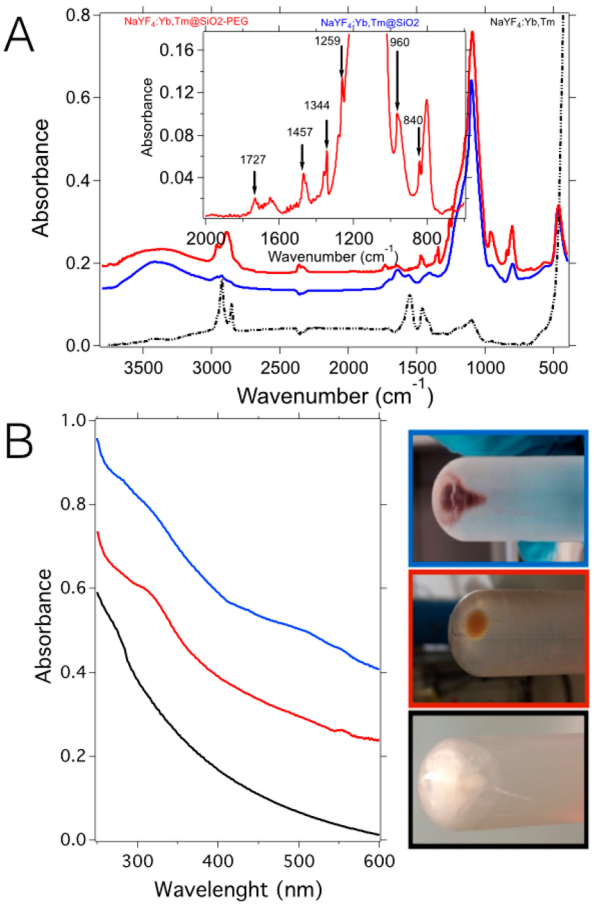

Figure 2. A) FTIR spectra of $NaYF_4$:Yb,Tm (dotted black line), $NaYF_4$:Yb,Tm@SiO_2 (blue line), and $NaYF_4$:Yb,Tm@SiO_2-PEG (red line). The inset depicts a magnification of $NaYF_4$:Yb,Tm@SiO_2-PEG spectra in the region comprised between 2000 and 400 cm^{-1}. B) UV–vis spectra of the bare UCNP@SiO_2-PEG (black), *o*-NBA functionalized UCNP@SiO_2-PEG (red), and Dox loaded UCNP@SiO_2-PEG (blue). The insets in the right show the aspect of the nanoparticles after the centrifugation.

nanoparticles presented the characteristic bands between 2900 and 2700 cm^{-1} due to existence of CH_2 and CH_3 groups and two bands at 1558 and 1403 cm^{-1}, which corresponded to the asymmetric and symmetric stretching vibration of the COO^- groups, respectively. These bands were attributed to the presence of oleic acid as capping agent on the surface of the nanoparticles. After coating the $NaYF_4$:Yb,Tm nanoparticles with SiO_2, the spectrum showed the characteristic absorption peaks of silica located at 1100, 935, and 750 cm^{-1}, which were attributed to the asymmetric stretching of the Si–O–Si, asymmetric stretching of Si–OH, and the symmetric stretching of the Si–O–Si, respectively. After grafting the PEG chains, the FTIR spectrum of these nanoparticles depicted new bands located at 1452, 1344, 1259, 960, and 840 cm^{-1} as well as an increment of the intensity of those bands localized between 3000 and 2800 cm^{-1}, which were attributed to the presence of the PEG chains.

After this step, the surface was functionalized with the photodegradable *o*-NBA derivate, which was synthesized as a bifunctional molecule capable of reacting with the surface of the UCNP@SiO_2 nanoparticles on one side and serving as an anchoring point for the Dox on the other side. The attachment of the *o*-NBA derivates produced a variation in the UV–vis spectrum of the UCNPs@SiO_2-PEG nanoparticles, which showed a new absorption band around 345 nm. Subsequently, Dox was linked to the acrylate moiety of the *o*-NBA by the thiol–acrylate Michael addition reaction.[35] As result, the UV–vis spectrum of the Dox-loaded UCNP@SiO_2 showed a new absorption band at 480 nm, which corresponded to the anchored Dox. A control experiment was carried out to check whether Dox could be physisorbed on the silica. For that, $NaYF_4$:Yb,Tm@SiO_2 nanoparticles without *o*-NBA were incubated overnight with thiolated Dox. After the cleaning process the UV–vis spectra of the precipitate did not show the presence of Dox. Figure 2B depicts the UV–vis absorption spectra of the UCNP@SiO_2 after attaching the *o*-NBA and the Dox.

The loading capacity experiment permitted to infer that the Dox payload of the nanoparticles was 1.4% in weight.

The UCNP@SiO_2 nanoparticles emitted multicolor NIR to UV–vis upconversion fluorescence when they were excited with a 980 nm laser, as shown in Figure 3A. The emission

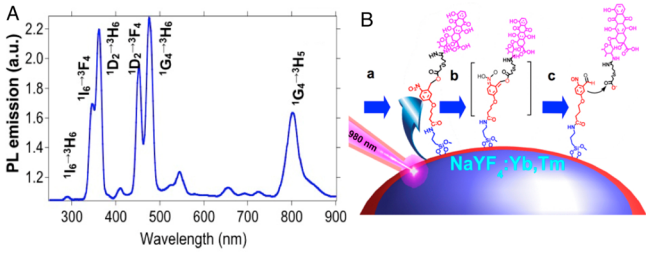

Figure 3. A) Photoluminescence emission spectra of the UCNPs using a 980 nm laser as excitation source. B) Scheme of the mechanism involved in the Dox delivery after NIR light illumination. Upon illumination with a NIR laser beam, the UCNP would emit photons in the UV region (345 and 365 nm) (a), which could be absorbed by the o-NBA molecules anchored on the surface of the UCNPs (b). The absorption of these photons would initiate the molecule degradation, releasing the Dox anchored on it (c).

bands at 345 and 365 nm overlapped with the absorption band of the *o*-NBA, which triggered the photodegradation of the *o*-NBA, releasing the anchored Dox. This could be used to control the drug release and to focus the pharmacological effect on a specific zone, where the light stimulus can be precisely located. Figure 3B depicts the action mechanism that could be involved in the drug release upon NIR irradiation.

The mechanism involved in the *o*-NBA degradation and the drug release consists of three stages as described by Wirz et al.[26] In the first stage, the emitted UV photons (λ = 345–365 nm) would be absorbed by the photodegradable *o*-NBA linkers. In a second stage, cyclization is assumed to proceed irreversibly, and only from the *neutral* nitronic acid, which is formed by pre-equilibrium protonation of the *aci*-anion. Finally, in the third stage, ring opening and elimination reactions lead to the Dox release, see Figure 3B.

The NIR triggered drug release was tested with different samples of Dox-loaded UCNP@SiO_2 nanoparticles that were irradiated with a 980 nm laser beam with an intensity of 6.3 W/

DOI: 10.1021/acsami.5b03881
ACS Appl. Mater. Interfaces 2015, 7, 14992–14999

cm^2 for different periods of time. Figure 4A shows the fluorescence spectra obtained from the supernatants after

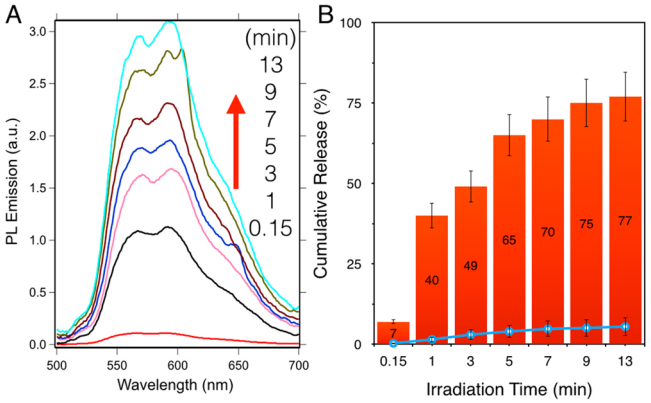

Figure 4. A) PL emission spectra of the supernatants (λ_{exc}= 475 nm) obtained after exposing the samples to a 980 nm laser with an intensity of 6.3 W/cm^2 for different periods of time ranging from 0.15 to 13 min. B) Cumulative release in percentage of Dox as a function of the irradiation time (bars) and in the absence of the NIR stimulus (blue points).

different irradiation times. The cumulative release of Dox as a function of the irradiation time is depicted in Figure 4B. In this later case, the cumulative amount of Dox released from the UCNPs in the absence of NIR light was tested as control experiment (blue points in Figure 4B). Without NIR irradiation the released Dox was less than 3% of the entire payload after 13 min.

These experiments indicated that upon illumination with a 980 nm laser, the Dox-loaded UCNP@SiO_2 nanoparticles were able to release the drug. The amount of released Dox increased significantly when the system was exposed to the NIR laser for longer periods of time. This result indicates that effectively the driven force of the releasing mechanism would be the photolysis of *o*-NBA. In contrast, a negligible amount of drug was observed without NIR irradiation, indicating that the Dox remained anchored in the absence of stimulus, which is of vital importance to avoid the uncontrolled release.

To study whether the proposed system could be effectively used as a drug delivery system triggered by NIR light we performed *in vitro* studies with HeLa cells. First, we tested the influence of the NIR radiation on the cell viability exposing the HeLa cells to a 980 nm laser for 5 min. These experiments demonstrated that the NIR light stimulus did not affect the cell viability, as shown in Figure 5A.

The IC_{50} of free Dox was determined in HeLa cells as shown in Figure 5B. This experiment revealed that IC_{50} of Dox in HeLa cells was 0.12 μg/mL.

Two of the most important studies that we boarded in this work were to determine the inherent cytotoxicity of the UCNP@SiO_2 nanoparticles and the influence of the emitted UV light from UCNP@SiO_2. For that, different amounts of UCNP@SiO_2 nanoparticles were cultured with HeLa cells. A group of plates were exposed to the NIR light stimulus, while another group was not irradiated. As shown in Figure 6, the viability of the cells treated with UCNP@SiO_2 and NIR laser and those treated with bare UCNP@SiO_2 without NIR laser showed low cytotoxicity, even after 48 h of incubation with concentrations of nanoparticles as high as 100 μg/mL. These experiments showed that under our experimental conditions,

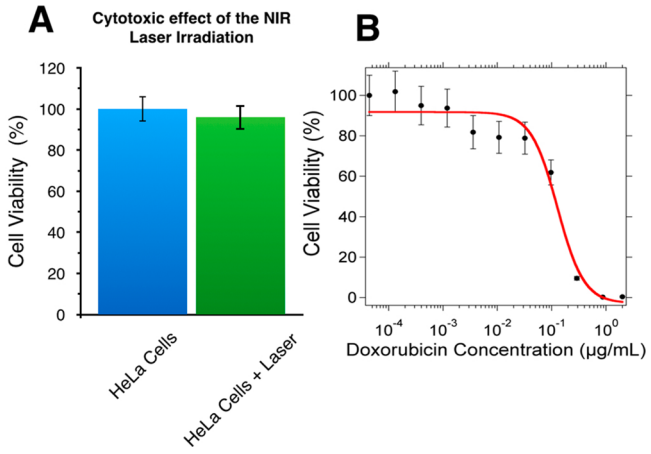

Figure 5. A) Cell viability of HeLa cultures after being exposed to a 980 nm laser beam for 5 min. B) Cell viability of HeLa cultures as a function of different concentrations of free Dox.

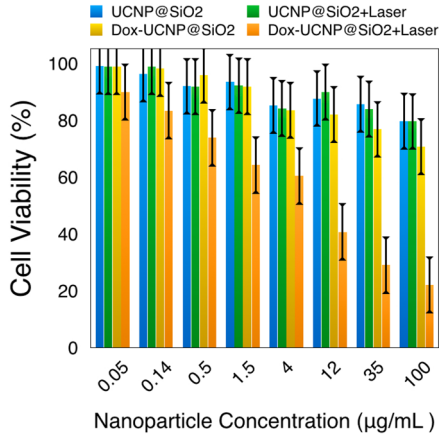

Figure 6. Cell viability of HeLa cells after 48 h of incubation in the presence of different concentrations of UCNP@SiO_2 and Dox-loaded UCNP@SiO_2 nanoparticles with or without the 5 min NIR light stimulus.

not only the NIR light but also the upconverted UV radiation did not influence significantly on the cell viability. The low cytotoxicity of the upconverted UV light might be attributed to the short exposition time of the experiments, which was 5 min just after pouring the UCNP@SiO_2 nanoparticles in the cell cultures. This could limit substantially the toxic effect of the UV radiation, since during the NIR exposure the UV light would not be emitted within the cells.[36]

Interestingly, when we examined the effect of the Dox-loaded UCNP@SiO_2 nanoparticles without being exposed to the NIR light stimulus, we observed a low cytotoxic effect, which augmented when the concentration of the nanoparticles was increased. This result would indicate that the effective Dox concentration was highly reduced when the drug was covalently attached to the surface of the nanoparticles. As result, in the absence of stimulus the effect of the drug would be minimized, allowing the reduction of side effects.

By contrast, when the cells were cultured with Dox-loaded UCNP@SiO_2 nanoparticles and exposed to the NIR light, the cell viability was reduced progressively as the nanoparticle concentration increased, showing a cell viability of 21% at a concentration of 100 μg/mL. From this result, we could infer an IC_{50} for the Dox-loaded UCNP@SiO_2 nanoparticles ca. 12

DOI: 10.1021/acsami.5b03881
ACS Appl. Mater. Interfaces 2015, 7, 14992−14999

μg/mL. This concentration would release about 0.11 μg/mL of Dox, which is in the order of magnitude of the IC_{50} measured for free Dox (0.12 μg/mL), see Figure 6. This result demonstrated that upon the NIR light illumination, the nanoparticles released active Dox to the medium, reaching a therapeutic concentration that reduced significantly the HeLa cell viability.

These results suggest that the proposed system is functional, since it showed low cytotoxicity in the absence of the light stimulus and a remarkable therapeutic effect in the presence of the stimulus.

CONCLUSIONS

A new kind of Dox-loaded $NaYF_4$:Yb,Tm@SiO_2 nanosystem has been successfully prepared. The surface of the nanoparticles was conveniently modified with PEG and a photodegradable linker based on *o*-NBA. The Dox was bound to the photodegradable linker remaining attached to the surface of the nanoparticles. The obtained material showed upconversion fluorescence when it was exposed to a NIR (980 nm) laser, emitting UV photons at 345 and 365 nm. These upconverted photons were able to trigger the degradation of the photodegradable linker, releasing the Dox. This phototriggered drug delivery system was tested "in vitro" on HeLa cells, evaluating the cell viability via the MTT assay. The results of this study showed that effectively the Dox-loaded UCNP@SiO_2 nanoparticles provoked cytotoxic effects on the HeLa cells when they were exposed to NIR light. This cytotoxic effect was dependent on the concentration of nanoparticles. In addition, the cytotoxic effect was not observed in the absence of NIR light or absence of Dox, which demonstrated the capability of the proposed system to minimize the side effects of highly toxic drugs, which would have potential application in cancer therapy.

ASSOCIATED CONTENT

Supporting Information

UV−vis, ^{1}H NMR, EDX, and FT-IR spectra, X-ray pattern, detailed TEM micrographs, and a standard linear calibration curve of Dox. The Supporting Information is available free of charge on the ACS Publications website at DOI: 10.1021/acsami.5b03881.

AUTHOR INFORMATION

Corresponding Author

*E-mail: bjrubio@ucm.es.

Notes

The authors declare no competing financial interest.

ACKNOWLEDGMENTS

Mineco for the grants MAT2014-55065R and BIO2013-42984R and Comunidad de Madrid for the Grant S2010/BMD-2457 are gratefully acknowledged. P.A.C. acknowledges the Spanish Ministry of Education for FPU Grant No. AP2010-1163. E.L.C. would also like to thank the EU COST action CM1101. We wish to thank Ailyn Martinez for her technical assistance.

REFERENCES

(1) Du, J.; Du, X.; Mao, C.; Wang, J. Tailor-Made Dual pH-Sensitive Polymer-Doxorubicin Nanoparticles for Efficient Anticancer Drug Delivery. *J. Am. Chem. Soc.* **2011**, 17560−17563.

(2) Dai, Y.; Ma, P.; Cheng, Z.; Kang, X.; Zhang, X.; Hou, Z.; Li, C. Up-Conversion Cell Imaging and pH- Induced Thermally Controlled Drug Re Lease from NaYF4:Yb3+/Er3+@Hydrogel Core-Shell Hybrid Microspheres. *ACS Nano* **2012**, *6*, 3327−3338.

(3) You, J.; Zhang, G.; Li, C. Exceptionally High Payload of Doxorubicin in Hollow Gold Nanospheres for Near-Infrared Light-Triggered Drug Release. *ACS Nano* **2010**, *4*, 1033−1041.

(4) Satarkar, N. S.; Biswal, D.; Hilt, J. Z. Hydrogel Nanocomposites: A Review of Applications as Remote Controlled Biomaterials. *Soft Matter* **2010**, *6*, 2364−2371.

(5) Tang, L.; Gabrielson, N. P.; Uckun, F. M.; Fan, T. M.; Cheng, J. Size-Dependent Tumor Penetration and In Vivo Efficacy of Monodisperse Drug-Silica Nanoconjugates. *Mol. Pharmaceutics* **2013**, *10*, 883−892.

(6) Wu, E. C.; Park, J. H.; Park, J.; Segal, E.; Cunin, F.; Sailor, M. J. Oxidation-Triggered Release of Fluorescent Molecules or Drugs from Mesoporous Si Microparticles. *ACS Nano* **2008**, *2*, 2401−2409.

(7) Gai, S.; Yang, P.; Li, C.; Wang, W.; Dai, Y.; Niu, N.; Lin, J. Synthesis of Magnetic, Up-Conversion Luminescent, and Mesoporous Core-Shell-Structured Nanocomposites as Drug Carriers. *Adv. Funct. Mater.* **2010**, *20*, 1166−1172.

(8) Serrano-Ruiz, D.; Laurenti, M.; Ruiz-Cabello, J.; López-Cabarcos, E.; Rubio-Retama, J. Hybrid Microparticles for Drug Delivery and Magnetic Resonance Imaging. *J. Biomed. Mater. Res., Part B* **2013**, *101*, 498−505.

(9) Ruiz-Hernández, E.; Baeza, A.; Vallet-Regí, M. Smart Drug Delivery through DNA/magnetic Nanoparticle Gates. *ACS Nano* **2011**, *5*, 1259−1266.

(10) Weaver, C.; LaRosa, J.; Luo, X.; Cui, X. Electrically Controlled Drug Delivery from Graphene Oxide Nanocomposite Films. *ACS Nano* **2014**, *8*, 1834−1843.

(11) Alvarez-lorenzo, C.; Bromberg, L.; Concheiro, A. Review Light-Sensitive Intelligent Drug Delivery Systems. *Photochem. Photobiol.* **2009**, *85*, 848−860.

(12) Yuan, Q.; Zhang, Y.; Chen, T.; Lu, D.; Zhao, Z.; Zhang, X.; Li, Z. Photon-Manipulated Drug Release from a Mesoporous Nanocontainer Controlled by Azobenzene-Modified Nucleic Acid. *ACS Nano* **2012**, 6337−6344.

(13) Liu, J.; Bu, W.; Pan, L.; Shi, J. NIR-Triggered Anticancer Drug Delivery by Upconverting Nanoparticles with Integrated Azobenzene-Modified Mesoporous Silica. *Angew. Chem., Int. Ed.* **2013**, *52*, 4375−4379.

(14) Son, S.; Shin, E.; Kim, B.-S. Light-Responsive Micelles of Spiropyran Initiated Hyperbranched Polyglycerol for Smart Drug Delivery. *Biomacromolecules* **2014**, *15*, 628−634.

(15) Chien, Y.; Chou, Y.; Wang, S.; Hung, S.; Liau, M.; Chao, Y. Near-Infrared Light Photocontrolled Chemotherapy with Caged Upconversion Nanoparticles in Vitro and in Vivo. *ACS Nano* **2013**, *7*, 8516−8528.

(16) Griffin, D. R.; Kasko, A. M. Photodegradable Macromers and Hydrogels for Live Cell Encapsulation and Release. *J. Am. Chem. Soc.* **2012**, *134*, 13103−13107.

(17) Luo, Y.-L.; Shiao, Y.-S.; Huang, Y.-F. Release of Photoactivatable Drugs from Plasmonic Nanoparticles for Targeted Cancer Therapy. *ACS Nano* **2011**, *5*, 7796−7804.

(18) Ju, E.; Li, Z.; Liu, Z.; Ren, J.; Qu, X. Near-Infrared Light-Triggered Drug-Delivery Vehicle for Mitochondria-Targeted Chemo-Photothermal Therapy. *ACS Appl. Mater. Interfaces* **2014**, *6*, 4364−4370.

(19) Yan, B.; Boyer, J. C.; Habault, D.; Branda, N. R.; Zhao, Y. Near Infrared Light Triggered Release of Biomacromolecules from Hydrogels Loaded with Upconversion Nanoparticles. *J. Am. Chem. Soc.* **2012**, *134*, 16558−16561.

(20) Wang, F.; Deng, R.; Wang, J.; Wang, Q.; Han, Y.; Zhu, H.; Chen, X.; Liu, X. Tuning Upconversion through Energy Migration in Core-Shell Nanoparticles. *Nat. Mater.* **2011**, *10*, 968−973.

(21) Sedlmeier, A.; Achatz, D. E.; Fischer, L. H.; Gorris, H. H.; Wolfbeis, O. S. Photon Upconverting Nanoparticles for Luminescent Sensing of Temperature. *Nanoscale* **2012**, *4*, 7090−7096.

DOI: 10.1021/acsami.5b03881
ACS Appl. Mater. Interfaces 2015, 7, 14992−14999

(22) Cui, S.; Yin, D.; Chen, Y.; Di, Y.; Chen, H.; Ma, Y.; Achilefu, S. In Vivo Targeted Deep-Tissue Photodynamic Therapy Based on Near-Infrared Light Triggered Upconversion Nanoconstruct. *ACS Nano* **2013**, *7*, 676−688.
(23) Hao, S.; Chen, G.; Yang, C. Sensing Using Rare-Earth-Doped Upconversion Nanoparticles. *Theranostics* **2013**, *3*, 331−345.
(24) Dai, Y.; Xiao, H.; Liu, J.; Yuan, Q.; Ma, P.; Yang, D.; Li, C.; Cheng, Z.; Hou, Z.; Yang, P.; et al. In Vivo Multimodality Imaging and Cancer Therapy by Near-Infrared Light-Triggered Trans-Platinum Pro-Drug-Conjugated Upconverison Nanoparticles. *J. Am. Chem. Soc.* **2013**, *135*, 18920−18929.
(25) Zhao, H.; Sterner, E. S.; Coughlin, E. B.; Theato, P. O-Nitrobenzyl Alcohol Derivatives: Opportunities in Polymer and Materials Science. *Macromolecules* **2012**, 1723−1736.
(26) Pelliccioli, A. P.; Wirz, J. Photoremovable Protecting Groups: Reaction Mechanisms and Applications. *Photochem. Photobiol. Sci.* **2002**, *1*, 441−458.
(27) Fedoryshin, L. L.; Tavares, A. J.; Petryayeva, E.; Doughan, S.; Krull, U. J. Near-Infrared-Triggered Anticancer Drug Release from Upconverting Nanoparticles. *ACS Appl. Mater. Interfaces* **2014**, *27*, 13600−13606.
(28) Li, Z.; Zhang, Y. An Efficient and User-Friendly Method for the Synthesis of Hexagonal-Phase NaYF(4):Yb, Er/Tm Nanocrystals with Controllable Shape and Upconversion Fluorescence. *Nanotechnology* **2008**, *19* (345606), 1−5.
(29) Serrano-Ruiz, D.; Alonso-Cristobal, P.; Mendez-Gonzalez, D.; Laurenti, M.; Olivero-David, R.; López-Cabarcos, E.; Rubio-Retama, J. Nanosegregated Polymeric Domains on the Surface of Fe3O4@SiO2 Particles. *J. Polym. Sci., Part A: Polym. Chem.* **2014**, *52*, 2966−2975.
(30) Han, Y.; Jiang, J.; Lee, S. S.; Ying, J. Y. Reverse Microemulsion-Mediated Synthesis of Silica-Coated Gold and Silver Nanoparticles. *Langmuir* **2008**, 5842−5848.
(31) Vaz, A. M.; Serrano-Ruiz, D.; Laurenti, M.; Alonso-Cristobal, P.; Lopez-Cabarcos, E.; Rubio-Retama, J. Synthesis and Characterization of Biocatalytic Γ-Fe2O3@SiO2 Particles as Recoverable Bioreactors. *Colloids Surf., B* **2014**, *114*, 11−19.
(32) Alonso-Cristobal, P.; Laurenti, M.; Sanchez-Muniz, F. J.; López-Cabarcos, E.; Rubio-Retama, J. Polymeric Nanoparticles with Tunable Architecture Formed by Biocompatible Star Shaped Block Copolymer. *J. Polym. Sci., Part A: Polym. Chem.* **2012**, *53*, 4569−4578.
(33) Li, G.-Z.; Randev, R. K.; Soeriyadi, A. H.; Rees, G.; Boyer, C.; Tong, Z.; Davis, T. P.; Becer, C. R.; Haddleton, D. M. Investigation into Thiol-(meth)acrylate Michael Addition Reactions Using Amine and Phosphine Catalysts. *Polym. Chem.* **2010**, *1*, 1196−1204.
(34) Greenfield, R. S.; Kaneko, T.; Daues, A.; Edson, M. A.; Fitzgerald, K. A.; Olech, L. J.; Grattan, A.; Spitalny, G. L.; Braslawsky, G. R. Evaluation in Vitro of Adriamycin Immunoconjugates Synthesized Using an Acid-Sensitive Hydrazone Linker Evaluation in Vitro of Adriamycin Immunoconjugates Synthesized Using an Acid-Sensitive Hydrazone Linker. *Cancer Res.* **1990**, *50*, 6600−6607.
(35) Carling, C. J.; Nourmohammadian, F.; Boyer, J. C.; Branda, N. R. Remote-Control Photorelease of Caged Compounds Using Near-Infrared Light and Upconverting Nanoparticles. *Angew. Chem., Int. Ed.* **2010**, *49*, 3782−3785.
(36) Li, W.; Wang, J.; Ren, J.; Qu, X. Near-Infrared Upconversion Controls Photocaged Cell Adhesion. *J. Am. Chem. Soc.* **2014**, *136*, 2248−2251.
(37) Dongmei, Y.; Ping'an, Ma.; Zhiyou, H.; Ziyong, C.; Chunxia, L.; Jun, L. Current Advances in Lanthanide Ion (Ln3+)-based Upconversion Nanomaterials for Drug Delivery. *Chem. Soc. Rev.* **2015**, *44*, 1416−1448.

DOI: 10.1021/acsami.5b03881
ACS Appl. Mater. Interfaces 2015, 7, 14992−14999